RESEARCH

Quasi-4-dimension ionospheric modeling and its application in single-frequency PPP

Shengfeng Gu[1*], Chengkun Gan[1], Chengpeng He[1], Haixia Lyu[1], Manuel Hernández-Pajares[2], Yidong Lou[1], Jianghui Geng[1] and Qile Zhao[1]

*Correspondence: gsf@whu.edu.cn
[1]GNSS Research Center, Wuhan University, 129 Luoyu Road Wuhan 430079 China
Full list of author information is available at the end of the article

Abstract

Ionospheric delay modeling is not only important for GNSS based space weather study and monitoring, but also an efficient tool to overcome the long convergence time of PPP. In this study, a novel model, denoted as Q4DIM (Quasi-4-dimension ionospheric modeling) is proposed for wide-area high precision ionospheric delay correction. In Q4DIM, the LOS (line of sight) ionospheric delay from a GNSS station network is divided into different clusters according to not only latitude and longitude, but also elevation and azimuth. Both GIM (global ionosphere map) and SID (slant ionospheric delay) that traditionally used for wide-area and regional ionospheric delay modeling, respectively, can be regarded as special case of Q4DIM by defining proper grids in latitude, longitude, elevation and azimuth. Thus, Q4DIM presents a resilient model that is capable for both wide-area coverage and high precision. Then four different sets of clusters are defined to illustrate the properties of Q4DIM based on 200 EPN stations. The results suggested that Q4DIM is compatible with the widely acknowledged GIM products. Moreover, it is proved that by inducting the elevation and azimuth angle dependent residuals, the precision of the 2-dimensional GIM-like model, i.e., Q4DIM-2D, is improved from around 1.5 TECU to better than 0.5 TECU. In addition, by treating Q4DIM as a 4-dimensional matrix in latitude, longitude, elevation and azimuth, its sparsity is less than 5%, thus guarantees its feasibility in a bandwidth-sensitive applications, e.g., satellite-based PPP-RTK service. Finally, the advantage of Q4DIM in single frequency PPP over the 2-dimensional models is demonstrated with one month's data from 30 EPN stations.

Keywords: Undifferenced and uncombined observation, Ionosphere delay modeling, PPP, DESIGN, Wide-area

1 Introduction

With the development of GPS, GLONASS, Galileo and BDS, Global Navigation Satellite System (GNSS) plays an important role in the positioning, navigation and timing (PNT) nowadays, especially for the high-precision applications [Teunissen and Montenbruck (2017), Yang et al. (2020)]. By taking the advantage of cost-efficiency, flexibility and global coverage into consideration, the precise point positioning (PPP) proposed by [Zumberge et al. (1997)] has been evolving into one of the most promising techniques in both science and engineering. e.g., earthquake and tsunami early warning, GNSS-based weather forecasting and navigation, etc. [Kouba and Héroux (2001), Guerova et al. (2016), Yigit and Gurlek (2017)]. However, compared with the traditional real-time kinematic (RTK) technique, the popularization of PPP in real-time (RT) applications was hindered by its long convergence time of typically 30 minutes.

To overcome this problem, [Gabor and Nerem (1999)] presented the first work to perform integer ambiguity resolution (AR) in PPP with single difference (SD) observation. The key point is that the fractional-cycle part of the carrier phase ambiguity that destroyed its integer property should be estimated from a network for each satellite, and then applied to the users to enable its AR [Geng et al. (2019A)]. Based on this principle, different models, e.g., uncalibrated phase delay (UPD), integer clock and decoupled clock, et al. were developed since then [Ge et al. (2008), Laurichesse et al. (2009), Collins et al. (2010)]. In addition, recent advances in multi-frequency multi-GNSS data processing have paved the way for a more reliable and efficient AR in PPP [Gu et al. (2015A), Geng et al. (2019B), Zhao et al. (2021)]. The entire spectrum of these studies can be divided into two fundamental classes: first the optimal combination of multi-GNSS multi-frequency observation; second the signal bias modeling and correction for pseudo range and carrier phase. The first class includes numerous studies to find the basic observation for alternatives to the traditional ionosphere free (IF) combination that originally formulated for dual-frequency observation. Notably the undifferenced uncombined GNSS model in which the individual signal from variety of frequencies of multi-GNSS is incorporated in a single parameter estimation system directly, thus guarantees its flexibility in a multi-frequency multi-GNSS environment [Schönemann et al. (2011), Gu et al. (2015A)]. The second class mainly focuses on the bias calibration to align the signals generated from different channels, otherwise the hardware delay would lead to inconsistencies in multi-frequency multi-GNSS data processing [Hauschild and Montenbruck (2016), Lou et al. (2017)]. Among other benefits with increasing signals, partial ambiguity resolution (PAR) may be significantly improved in which a sufficiently large subset of ambiguities is selected instead of resolving the complete vector of integer ambiguities [Teunissen et al. (1999)]. [Psychas et al. (2021)] further argued that the contribution of multi-frequency observations in PPP AR is signicant and largely driven by frequency separation. However, even for multi-frequency multi-GNSS PPP with PAR, it still takes nearly 5 mins to get a position precision better than 10 cm [Psychas et al. (2020)].

Aside from multi-frequency multi-GNSS PAR, the constraint of a priori ionospheric information presented another way to accelerate PPP convergence, especially by taking the popularity of the undifferenced uncombined PPP model into consideration, in which the ionospheric delay cannot be eliminated as the IF model [Zhao et al. (2018)]. Obviously, the performance of the ionospheric delay model plays an important role in the ionosphere constrained undifferenced uncombined PPP (e.g. [Olivares-Pulido et al. (2021)]).

The worldwide distributed GNSS continuous operation reference station system (CORS) provide the measurement of total election content (TEC) with an unprecedented temporal and spatial resolution. Thus, GNSS is regarded as an excellent ionospheric sounding system nowadays. Attribute to the continued efforts of the Ionosphere working group (Iono-WG) within the IGS community, the global ionosphere maps (GIM) were independently generated on a regular basis by different ionospheric associate analysis centers (IAACs) since 1998 with a typical latency of several days [Schaer (1999), Li et al. (2012)]. To cope with the requirements of real-time (RT) GNSS data processing, IGS further issued a call for participation in IGS RT pilot project (IGS-RTPP) in 2007 [Caissy et al. (2012)], and over 200 IGS stations now provide real-time observation with a sampling rate of 1 Hz [Romero et al. (2018)]. More recently, several IAACs, including Centre National dÉtudes Spatiales (CNES), Chinese Academy of Sciences (CAS), Technical University of Catalonia (UPC-IonSAT) and Wuhan University (WHU) has begun to provide RT GIM products publicly by Networked Transport of RTCM (Radio Technical Commission for Maritime) via Internet Protocol (NTRIP) [Liu et al. (2021)]. Since then, a wide range of valuable literatures have been published concerning the precision evaluation of the GIM products [Hernández-Pajares et al. (2009), Ren et al. (2019)], as well as its performance in the applications of space weather monitoring and high precision positioning augmentation [Zhang et al. (2013), Hernández-Pajares et al. (2017)]. Depending on the stations involved, high and low solar activity, post-time and RT data processing, the results suggested that the precision of GIM usually varies from 2-8 TECU (1 TECU corresponding to 16 cm on GPS L1) [Wielgosz et al. (2021)]. Though these studies illustrated the efficiency of GIM in the ionospheric constrained PPP, especially for the single-frequency, the improvement is rather limited in the instantaneous convergence centimeter (cm) level positioning, i.e., PPP-RTK [Rovira-Garcia et al. (2015)].

An efficient way to improve the precision of ionospheric delay correction is to interpolate the slant ionospheric delay (SID) along LOS (line of sight) from a regional network for each satellite, and as demonstrated by [Teunissen et al. (2010)], this network-based PPP has the comparable performance with that of Network-RTK (NRTK). It should be noted, that the receiver biases would be absorbed by the ionospheric delay to remove the rank deficiency, thus special attention should be focused on the SID modeling for inconsistent receiver networks [Zhang et al. (2022)]. [Shi et al. (2012), Zhao et al. (2018)] presented a sophisticated ionospheric parameter constrain model, i.e., DEterministic plus Stochastic Ionosphere model for GNss (DESIGN), and it was demonstrated that the ionospheric delay can be separated from the receiver biases in this case [Gu et al. (2020), Zhang et al. (2021)]. Typically, the SID modeling performs much better than that of GIM since it uses the LOS ionospheric delay in modelling directly, thus avoiding the errors induced by the elevation mapping function and the constant-height thin-layer model [Li et al. (2017)]. Though the LOS ionospheric delay are highly correlated with each other for small station network, it can be hardly extended to wide-area ionospheric delay modeling. As a result, the networks involved in the above-mentioned study [Teunissen et al. (2010)] were rather small with a typical baseline length of around 15 km and 50 km, respectively.

In summary, both GIM and SID modeling are widely used nowadays with the purpose of wide-area coverage and high precision, respectively. In this study, we proposed a novel approach: Quasi-4-dimension ionospheric modeling (Q4DIM), that take the advantage of both. Besides the latitude and longitude factors in GIM modeling, the elevation and azimuth are further optionally taking into consideration in Q4DIM, thus both GIM and SID model can be regarded as a special case of Q4DIM with specified grid division approach along latitude, longitude, elevation and azimuth. In addition, it would be demonstrated that Q4DIM was rather sparse as a 4-dimension (optional) grid matrix, and the sparse storage technique was suggested to improve the efficiency. This paper is organized as follows: first, Q4DIM is introduced; then its property is analyzed by comparison with the GIM and SID model; finally, the performance of Q4DIM is assessed in single-frequency PPP with one month's data.

2 Q4DIM

As the estimation of LOS ionospheric delay from GNSS has been discussed in a wide range of publications, we start the Q4DIM with the set of LOS ionospheric delay directly. Concerning the details of GNSS ionospheric delay estimation of this work, we refer to the study of [Shi et al. (2012), Zhao et al. (2018)], in which the undifferenced and uncombined model constrained with DESIGN was utilized. Following this way, suppose that we have generated a set of LOS ionospheric delay with j satellites and k receivers

$$\boldsymbol{I} = \{I_r^s\} \qquad s.t. \qquad s \in (\ 1 \quad \cdots \quad j\ ), r \in (\ 1 \quad \cdots \quad k\ ) \tag{1}$$

Our purpose is to divide the whole set $\boldsymbol{I}$ into n pre-defined clusters $\boldsymbol{C} = \{C_i\}$ ($i \in (\ 1 \quad \cdots \quad n\ )$), and the ionospheric delay samples in each cluster are highly correlated with each other.

2.1 Algorithm

For a given network, we can select the grids in latitude, longitude, elevation and azimuth as

$$\left.\begin{array}{lcl} \boldsymbol{b} & = & (\ b_1 \quad \cdots \quad b_{n_b}\ ) \\ \boldsymbol{l} & = & (\ l_1 \quad \cdots \quad l_{n_l}\ ) \\ \boldsymbol{e} & = & (\ e_1 \quad \cdots \quad e_{n_e}\ ) \\ \boldsymbol{a} & = & (\ a_1 \quad \cdots \quad a_{n_a}\ ) \end{array}\right\} \tag{2}$$

where n_b, n_l, n_e, n_a is the number of grids in latitude, longitude, elevation and azimuth, respectively, which is selected to balance data volume and model precision according to the demand. Then, $\boldsymbol{b}, \boldsymbol{l}, \boldsymbol{e}, \boldsymbol{a}$ can be determined by uniform spatial subdivision for a given region and the selected number n_b, n_l, n_e, n_a directly. And there are

$$n = n_b \cdot n_l \cdot n_e \cdot n_a \tag{3}$$

clusters, and for the i-th cluster C_i, it is defined with its center point $\boldsymbol{o_i}$ as

$$C_i(\boldsymbol{o_i}) \quad s.t. \quad \boldsymbol{o_i} = (\ b_{i_b} \quad l_{i_l} \quad e_{i_e} \quad a_{i_a}\ )^T, i = (\ i_b \quad i_l \quad i_e \quad i_a\ ) \cdot \boldsymbol{ldm} \tag{4}$$

with $b_{i_b} \in \boldsymbol{b}, l_{i_l} \in \boldsymbol{l}, e_{i_e} \in \boldsymbol{e}, a_{i_a} \in \boldsymbol{a}$; $\boldsymbol{ldm} = \begin{pmatrix} l_b & l_l & l_e & l_a \end{pmatrix}^T$ denoted the leading dimension for latitude, longitude, elevation and azimuth, respectively

$$\left.\begin{array}{lcl} l_b & = & n_l \cdot n_e \cdot n_a \\ l_l & = & n_e \cdot n_a \\ l_e & = & n_a \\ l_a & = & 1 \end{array}\right\} \tag{5}$$

Recall the slant ionospheric delay I_r^s in Eq. (1), the corresponding LOS vector $\boldsymbol{los} = \begin{pmatrix} b & l & e & a \end{pmatrix}^T$ can be uniquely determined by the specific satellite s and receiver r, thus the set of slant ionospheric delay in Eq. (1) can be rewritten as $\boldsymbol{I} = \{I_{los}\}$. Then with the clusters defined by Eq. (2) to (5), each I_{los} can be grouped into cluster C_i by iterating over the set $\boldsymbol{I}$

$$C_i \quad = \quad \{I_{los}\} \quad s.t. \quad \forall j \in \begin{pmatrix} 1 & \cdots & n \end{pmatrix} \rightarrow \|\boldsymbol{los} - \boldsymbol{o_i}\| \leq \|\boldsymbol{los} - \boldsymbol{o_j}\| \tag{6}$$

where $\| \cdot \|$ denotes the norm of the corresponding vector. Thus, for the cluster C_i, its averaged LOS ionospheric delay μ_i and standard deviation (STD) σ_i is derived as

$$\left.\begin{array}{lcl} \mu_i & = & \frac{1}{|C_i|} \sum I_{los} \\ \sigma_i & = & \sqrt{\frac{1}{|C_i|} \sum \left(I_{los} - I_{C_i}\right)^2} \end{array}\right\} \tag{7}$$

in which I_{los} and $|C_i|$ denotes the samples and the number of samples, respectively.

Up to now we have derived the numerical characteristics, i.e., μ_i, σ_i, for each cluster $C_i(\boldsymbol{o_i})$, and a straightforward way to represent the whole clusters is to view it as a large matrix. However, direct processing of the whole matrix is usually not applicable for its costliness due to a large amount of clusters. Moreover, it is also not necessary as the matrix is rather sparse, i.e., in most cases the number of samples of cluster $|C_i| = 0$, due to a limited distribution of both satellites and receivers, as would be demonstrated below. Thus, only those clusters with sufficient samples, e.g., $|C_i| \geq 2$, are retained in Q4DIM in a key-value form

$$C_{map} \quad : \quad i \quad - \quad \begin{pmatrix} \mu_i & \sigma_i \end{pmatrix} \tag{8}$$

Obviously, for the Q4DIM users, its cluster index i_u of a given LOS vector $\boldsymbol{los_u}$ can be obtained with Eq. (2) and (4), then the corresponding ionospheric delay corrections can be obtained by looking up the key-value map defined by Eq. (8). In addition, σ_i is the precision indicator for each cluster and can also be used for weighting in user ionospheric delay correction with Q4DIM, and we also defined the STD σ in Q4DIM as the averaged value of the STD for all cluster σ_i in Eq. (7)

$$\sigma = \frac{\sum_{i=1}^{n} \sigma_i}{n} \tag{9}$$

2.2 Discussion

Recall the grids in Eq. (2), the popular GIM model can be regarded as a special case of Q4DIM once the empty set was selected for both elevation and azimuth, i.e., $\boldsymbol{e} = \varnothing$, $\boldsymbol{a} = \varnothing$. However, since the sparse representation and processing technique is promoted in Q4DIM to improve its efficiency, the ionospheric delay correction is not available for all the grids as that of GIM. To overcome this dilemma, the LOS ionospheric delay is further suggested to be divided into deterministic and stochastic parts, i.e., $I_{los,0}$, r_{los}, as that of DESIGN [Shi et al. (2012), Zhao et al. (2018)]

$$I_{los} = I_{los,0} + r_{los} \tag{10}$$

while $I_{los,0}$ can be either interpolated from grids or calculated with the spherical harmonic function (SHF) of GIM. Then the set of ionospheric delay residual $\boldsymbol{r} = \{r_{los}\}$ can be grouped into different clusters and represented with a key-value map following the procedure in the algorithm section.

For the Q4DIM users, its ionospheric delay corrections of any LOS $\boldsymbol{los_u}$ is obtained as

$$I_{los_u} = I_{los_u,0} + \begin{cases} r_{los_u} & , \quad C_{map}(i_u) \neq \varnothing \\ 0 & , \quad C_{map}(i_u) = \varnothing \end{cases} \tag{11}$$

here again $I_{los_u,0}$ is either interpolated from grids or calculated with the SHF of GIM. Concerning the stochastic part r_{los_u}, the key i_u may exist in the Q4DIM map, then the ionospheric delay correction is further refined with the residual. Otherwise, the model is actually equivalent with GIM.

Besides the compatibility with GIM model, we further argued that the SID model, that is widely accepted in the regional network augmentation, is also a special case of Q4DIM model

$$\exists \boldsymbol{C} = \{C_i\} \quad s.t. \quad max(|C_i|) = 1 \quad \forall i \in \begin{pmatrix} 1 & \cdots & n \end{pmatrix} \tag{12}$$

in other words, a selection of clusters existed in which each cluster contains only one sample I_{los}/r_{los} at most. Then the key-value map actually consists of individual LOS ionospheric delay, i.e., SID model.

As a result, according to the grid definition in Eq. (2), Q4DIM presents a resilient model that is capable for both wide-area coverage and high precision

$$\underbrace{\boldsymbol{o_i} = \begin{pmatrix} b_{i_b} & l_{i_l} \end{pmatrix}^T}_{\text{GIM case}} \xleftarrow{\boldsymbol{e}=\varnothing,\boldsymbol{a}=\varnothing} \boldsymbol{C} = \{C_i(\boldsymbol{o_i})\} \xrightarrow[\text{defined sufficiently fine}]{\boldsymbol{b},\boldsymbol{l},\boldsymbol{e},\boldsymbol{a}} \underbrace{max(|C_i|) = 1}_{\text{SID case}} \tag{13}$$

Several statements should be emphasized here: First, though the LOS ionospheric delay is used in the algorithm derivation, we can also convert it to the vertical in Q4DIM without worrying about the mapping function error, as this error is elevation angle dependent, thus it can be compensated to a large extent with a similar elevation angle for each cluster in modeling and positioning. Second, we can use GIM / RT-GIM from IGS, or even the broadcast ionospheric models, e.g., KLOBUCHAR, as the deterministic ionospheric delay $I_{los,0}$ directly, and in this sense, Q4DIM is compatible with the existing model. In addition, the stochastic part r_{los_u} stands for the irregular spatial and temporal variations, and it is the key to improve the ionospheric delay precision, and typically it requires a much higher spatial-temporal resolution. Thus, by separate r_{los_u} from the large deterministic part, it can be represented with fewer data and consequently has the advantage to compress the data volume, which is of special importance for real-time service. Finally, we denoted the model as quasi-4-dimension since, that it is not a direct extension of the wide acknowledged 3-dimension model, i.e., the tomography ionospheric model. In addition, it may also be a two-dimension model like that of GIM as we have pointed out.

3 Experimental validation

To assess the performance of Q4DIM, the above algorithm is realized with the FUSING (FUSing IN Gnss) software and validated with single-frequency PPP (SF-PPP) in the following experiment. Up to now, FUSING is capable for real-time multi-GNSS precise orbit determination, satellite clock and bias estimation, atmosphere modeling and multi-sensor navigation [Gong et al. (2018), Shi et al. (2019), Luo et al. (2020), Gu et al. (2021)].

3.1 Data and strategy

The experiment is carried out with one month's data of EUREF Permanent Network (EPN). As shown in Fig. 1, the 200 stations in red are used for the Q4DIM, and the 30 stations in blue are used for SF-PPP. The observation are collected over the period of DOY (Day Of Year) 001 to DOY 030, 2020, with an interval of 30 seconds. The detail of the experiment is illustrated in Tab. 1. In addition, as presented in Tab. 2, four solutions for Q4DIM denoted as A, B, C and D with different grid definition are first compared. Then, the performance of Q4DIM in SF-PPP is assessed in terms of convergence time and precision.

Table 1 Details of the experiment

Item	Q4DIM	SF-PPP
Period	DOY 001 - 030, 2020	
System	GPS, Galileo	
Station	200 in red in Fig. 1	30 in blue in Fig. 1
Sampling	30 sec	
Weighting	0.2 m for pseudorange and 0.002 m for carrier phase Low elevation observable and outliers are down-weighted	
Ephemeris	Final orbit and clock product of Wuhan University	
PCO/PCV	Corrected with igs14.atx	
Ionosphere	DESIGN [Zhao et al. (2018)]	Q4DIM correction
Troposphere	GPT2 model with remaining estimated as a random walk process	
Ambiguity	Float constant for each continuous arc	

3.2 Comparison of Q4DIM

First, to get an intuitive impression of Q4DIM, we presented the LOS for the original SID, as well as LOS of each cluster, i.e., $\boldsymbol{o_i}$ in Eq. (4) for different solutions in Fig. 2. As we can see, by defining different clusters with Tab. 2, Q4DIM presents a

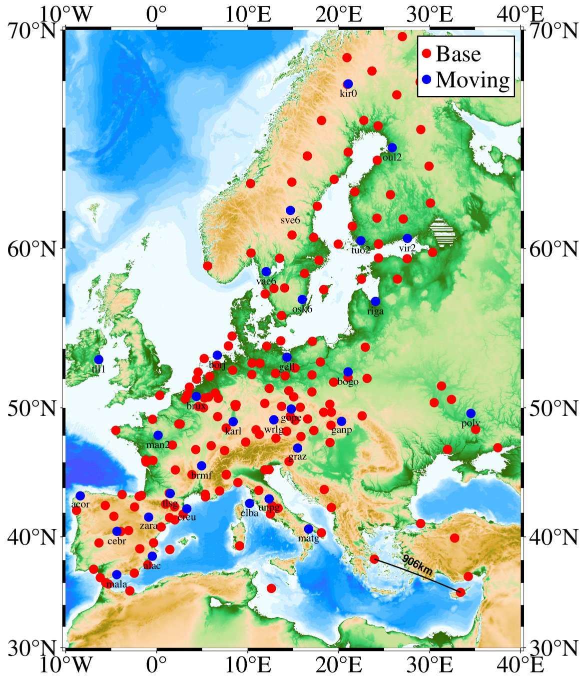

Figure 1 Distribution of 230 tracking stations over Europe, in which the red denoted 200 stations are used for Q4DIM, while the blue denoted 30 stations are used for single-frequency PPP

Table 2 Q4DIM strategy

Solution	n_b	n_l	n_e	n_a
A	12	8	6	25
B	24	16	12	50
C	36	24	18	75
D	48	32	24	100

rather flexible algorithm with resilient resolution and precision, that satisfies different requirement on modeling precision, coverage and data volume [Yang (2019)].

As we have pointed out, Q4DIM is a GIM-like 2-dimensional map once we ignore the residual part r_{los} in Eq. (10), denoted as Q4DIM-2D, and this is also the case that an empty set was selected for both elevation and azimuth, $\boldsymbol{e} = \varnothing, \boldsymbol{a} = \varnothing$. While the corresponding result is presented in Fig. 3 for different solutions. Recall Tab, 2, the number of grids over latitude and longitude is 12×8, 24×16, 36×24 and 48×32 for solution A, B, C and D, respectively. As expected, more details of ionospheric delay structure are revealed with a higher spatial resolution as illustrated in Fig. 3. Concerning the precision of different Q4DIM solutions, in Fig. 4 we presented the series of σ defined by Eq. (9) on DOY 001, 2020 as an example. As we can see, the precision can be hardly improved with the higher spatial resolution over latitude and longitude. This is reasonable since, that the errors in this case is most likely due to the mapping function and anisotropy. Actually, this result is in line with previous studies of GIM, in which it is suggested that the precision of 2-dimensional modeling can be hardly improved by increasing the degrees of SH function [Yuan et al. (2017), Zhao et al. (2018)].

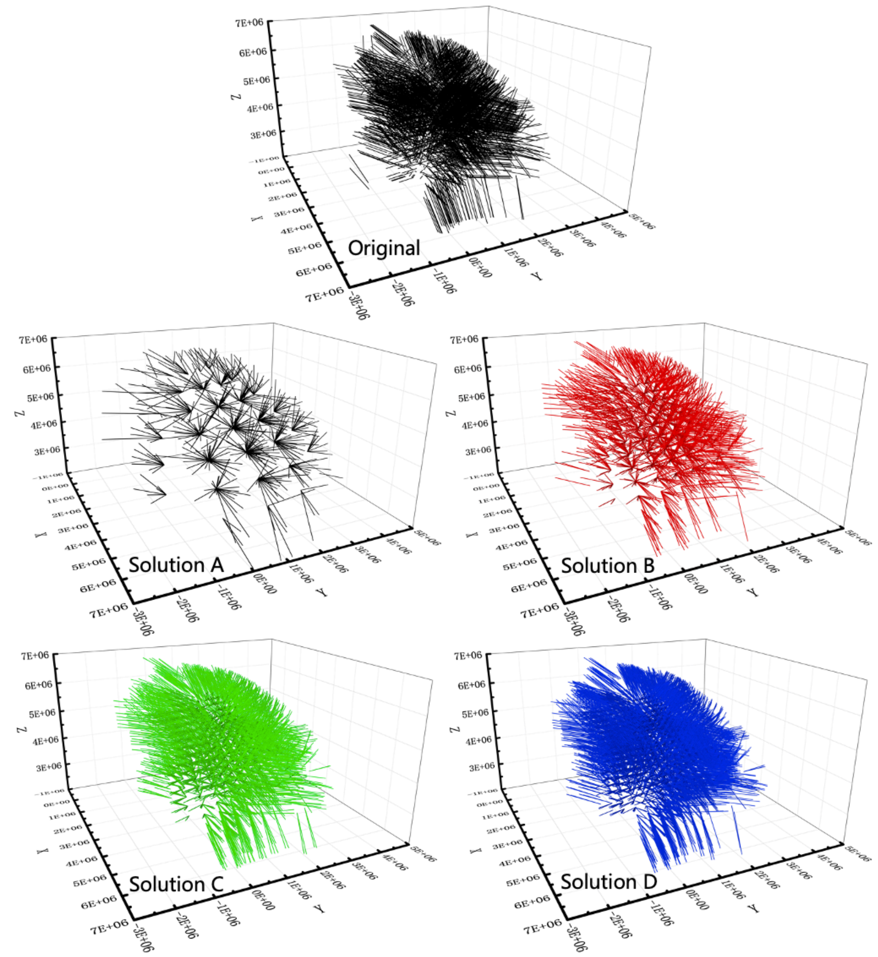

Figure 2 The LOS map for the original SID, and each clusters, i.e., $\boldsymbol{o}_i$ in Eq. (4) for solution A ($12 \times 8 \times 6 \times 25$), solution B ($24 \times 16 \times 12 \times 50$), solution C ($36 \times 24 \times 18 \times 75$) and solution D ($48 \times 32 \times 24 \times 100$)

To solve the above dilemma, Q4DIM introduces the residual ionospheric delay correction as Eq. (10) for each 2-dimensional grid, and the residual is further divided according to its elevation and azimuth angle. Selecting a latitude and longitude grid arbitrarily for each solution, Fig. 5 to 8 presented the distribution of the statistics defined by Eq. (7), i.e., number of samples $|C_i|$, averaged LOS ionospheric delay μ_i, and standard deviation σ_i, for each cluster. While the top two sub-plots present $|C_i|$, the left-bottom sub-plot presents μ_i, and the right-bottom sub-plot presents σ_i. Taking Fig. 5 of solution A as an example, for each 2-dimensional grid, it is further divided into 6×25 grids according to the elevation and azimuth angle. As indicated by the left-top sub-plot, the Q4DIM clusters are rather sparse as a 4-dimensional grid matrix since only a few grids have enough samples, i.e., $|C_i| \geq 2$. Thus, the left three sub-plots are enlarged for those grids with enough samples. From the left-bottom sub-plot, it is noted that the residuals μ_i for different grids varies from around -1.9 to 3.6 TECU, and they are exactly the errors in 2-dimensional TEC map in Fig. 4. By correcting these residuals, the precision can be improved significantly

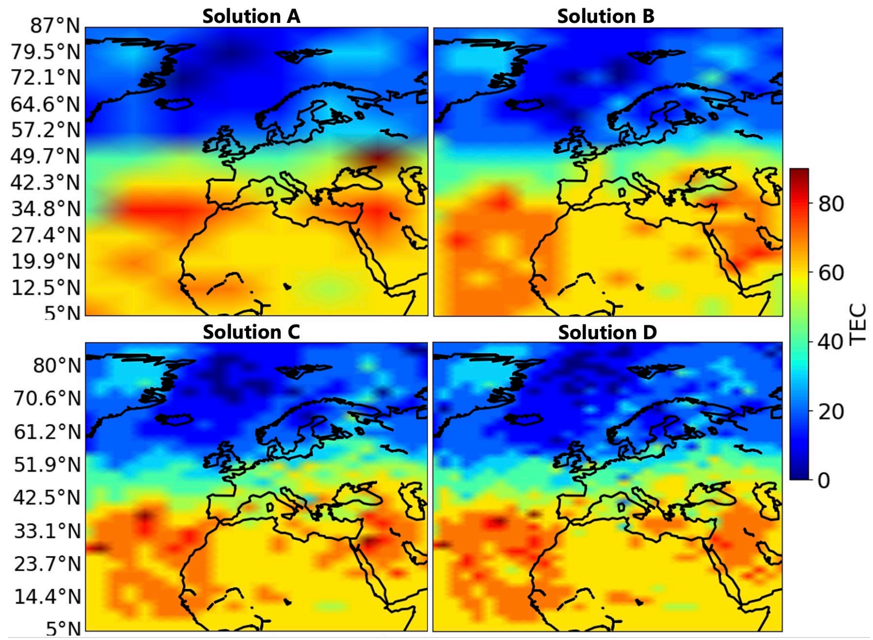

Figure 3 Distribution of the 2-dimensional TEC map with the resolution of 12×8, 24×16, 36×24, and 48×32 in latitude and longitude for Q4DIM-2D

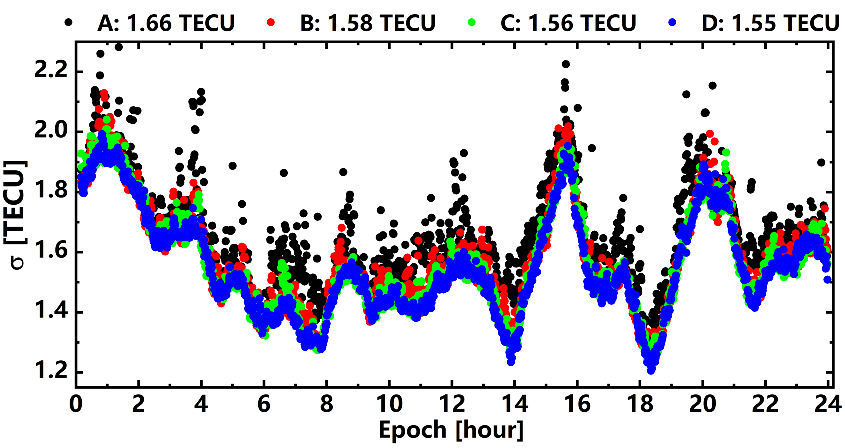

Figure 4 Series of σ in Eq. (9) for Q4DIM-2D TEC map of Solution A (black), Solution B (red), Solution C (green) and Solution D (blue) on DOY 001

as implied by the right-bottom sub-plot with σ_i less than 0.5 TECU. While, for solution B to solution D, a similar conclusion can be stated.

In Fig. 9 we further present the series of averaged STD σ in Eq. (9) for different solutions. As expected, with a higher resolution in the latitude, longitude, elevation and azimuth 4-dimensional space, the precision of Q4DIM improved from 0.46 TECU to 0.22 TECU. By comparison with the result in Fig. 4, it is argued that the ionospheric delay modeling precision can be improved significantly by taking elevation and azimuth into consideration. Besides the precision, the data volume is also a critical issue for the bandwidth-sensitive applications, e.g., satellite-based

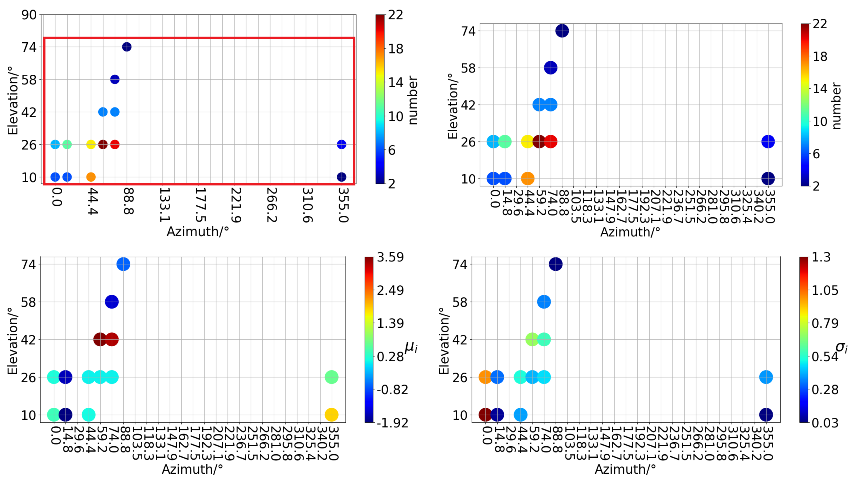

Figure 5 Distribution of $|C_i|, \mu_i, \sigma_i$ in Eq. (7) against elevation angle and azimuth angle for latitude $64.6°$ and longitude $40.7°$ of Solution A $(12 \times 8 \times 6 \times 25)$ on DOY 001

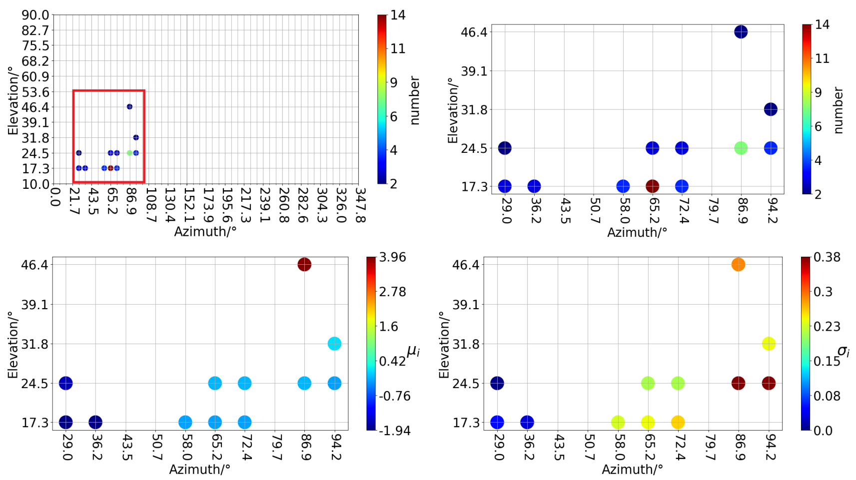

Figure 6 Distribution of $|C_i|, \mu_i, \sigma_i$ in Eq. (7) against elevation angle and azimuth angle for latitude $65.6°$ and longitude $41.7°$ of Solution B $(24 \times 16 \times 12 \times 50)$ on DOY 001

PPP-RTK service[Zhang et al. (2020)]. Fig. 5 to 8 already demonstrate that the 4-dimensional matrix is rather sparse. Thus, the middle two sub-plots of Fig. 9 show the series of the number of valid clusters, i.e., the clusters with $|C_i| \geq 2$, and the sparsity rate that defined as the ratio of the number of valid clusters over the total number of clusters n in Eq. (3). Taking solution B for instance, though there are 230400 clusters in total, the number of valid clusters is around 2100, and the sparsity rate is 0.9%. The results are rather promising and implied that the Q4DIM has the potential to be used for wide-area satellite-based augmentation service with a precision of better than 0.5 TECU. Finally, the bottom sub-plot gives the series of the LOS number for each valid cluster.

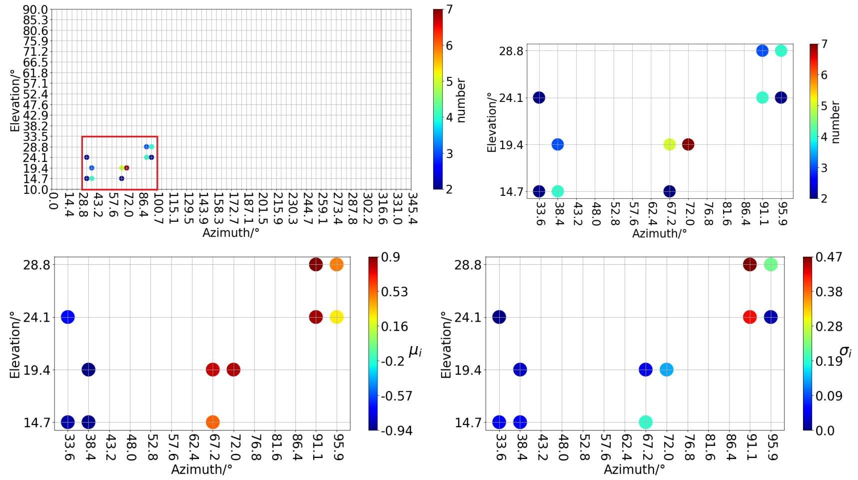

Figure 7 Distribution of $|C_i|, \mu_i, \sigma_i$ in Eq. (7) against elevation angle and azimuth angle for latitude $65.9°$ and longitude $42.0°$ of Solution C ($36 \times 24 \times 18 \times 75$) on DOY 001

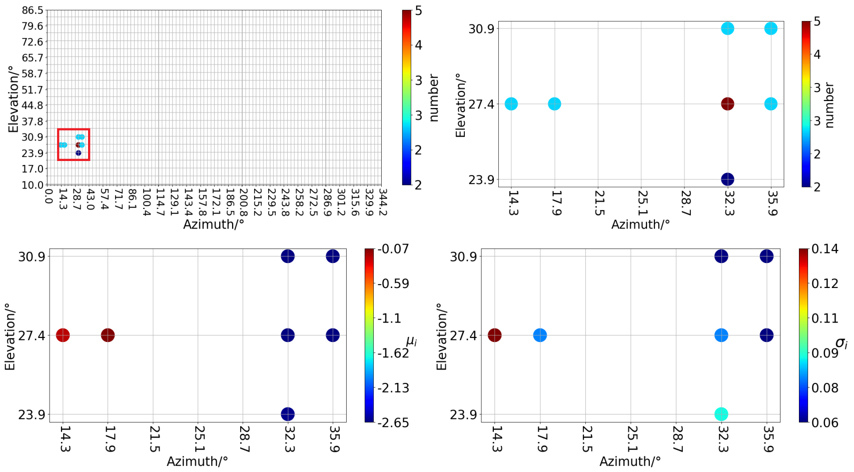

Figure 8 Distribution of $|C_i|, \mu_i, \sigma_i$ in Eq. (7) against elevation angle and azimuth angle for latitude $71.3°$ and longitude $32.4°$ of Solution D ($48 \times 32 \times 24 \times 100$) on DOY 001

3.3 SF-PPP

Based on the discussion in section 3.2, Q4DIM with solution B is selected and further validated in SF-PPP. The rover stations are denoted in blue as shown in Fig. 1. Four SF-PPP solutions are compared with different ionospheric delay elimination strategy as presented in Tab. 3. Though the stations are static, they are all processed in simulated kinematic model with a forward square root information filter (SRIF), and the filters are restarted every hour. Then the convergence serial in 68% confidence level convergence serial for DOY 001-030, 2020 of vertical (upper panel) and horizontal (bottom panel), respectively.

As we can see from Fig. 10, the SF-PPP solutions with undifferenced and uncombined observation constrained with DESIGN performs much better than that of the traditional GRAPHIC (Group and Phase Ionosphere Calibration) approach, and

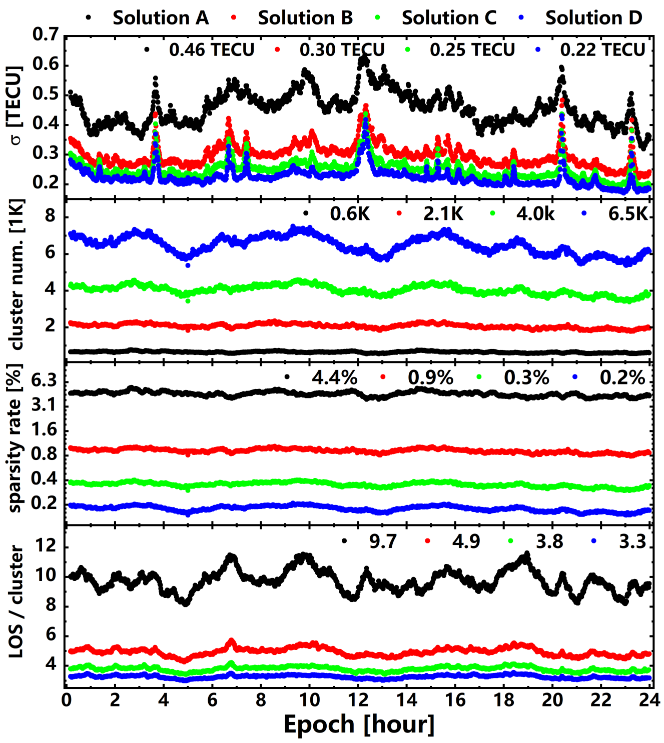

Figure 9 Time series of σ, number of valid clusters, sparsity rate and number of LOS per cluster for different Q4DIM solutions on DOY 001, 2020

Table 3 SF-PPP strategy

Solution	Ionospheric delay
IF	Eliminated with GRAPHIC combination [Shi et al. (2012)]
CODG	DESIGN with CODG GIM product as a priori correction model
Q4DIM-2D	DESIGN with Q4DIM-2D product as a priori correction model
Q4DIM	DESIGN with Q4DIM product as a priori correction model

the result is in line with our previous studies [Shi et al. (2012), Lou et al. (2015)]. In addition, though CODG and Q4DIM-2D are both 2-dimensional GIM-like ionospheric model, Q4DIM-2D performs better since more local stations are involved in the ionospheric delay modeling. While, Q4DIM performs best among all the ionospheric augmentation SF-PPP solutions in both vertical and horizontal, and its better performance over Q4DIM-2D demonstrate the advantage of elevation and azimuth angle division.

4 Conclusions

As the development of multi-frequency multi-GNSS, the ionospheric delay becomes one of the critical issues in the high precision data processing with undifferenced and uncombined model. Moreover, ionospheric delay augmentation is an efficient approach to accelerate PPP convergence. Thus, high precision ionospheric delay modeling has receiving increasing interests nowadays.

GIM and SID are the most popular ionospheric models in GNSS community, while each has merits and demerits. In this study, we proposed a novel ionospheric

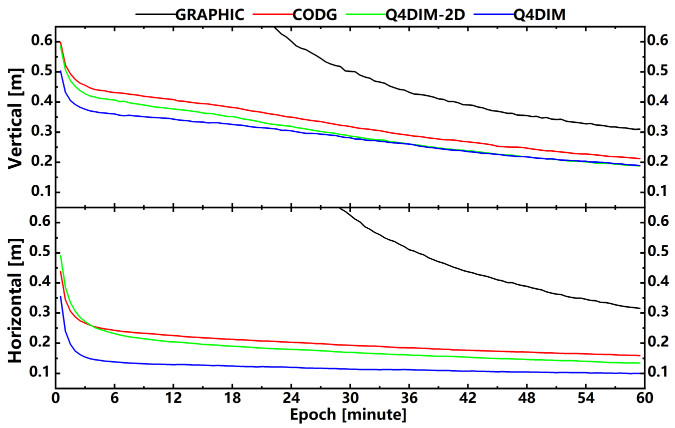

Figure 10 Single frequency PPP convergence serial in 68% confidence level for DOY 001-030, 2020 of vertical (upper panel) and horizontal (bottom panel), respectively. While for different ionospheric delay elimination strategies with GRAPHIC, CODG, Q4DIM-2D and Q4DIM, the results are denoted in black, red, green and blue, respectively

delay model, i.e., Q4DIM, that can take both the advantages of GIM and SID. In Q4DIM, the LOS ionospheric delay is divided into different clusters according to their latitude, longitude, elevation and azimuth. While, both GIM and SID can be regarded as special case of Q4DIM by defining the clusters properly. The properties of Q4DIM are discussed for four sets of clusters with different spatial resolution based on 200 EPN stations. The results suggest that by inducting the elevation and azimuth angle dependent residuals, the precision of the 2-dimensional GIM-like model, i.e., Q4DIM-2D, is improved from around 1.5 TECU to better than 0.5 TECU. In addition, treating Q4DIM as a 4-dimensional matrix in latitude, longitude, elevation and azimuth, it is rather sparse, thus guarantees its feasibility in a bandwidth-sensitive applications, e.g., satellite-based PPP-RTK service. Finally, the performance of Q4DIM and its advantage in SF-PPP over the 2-dimensional models are demonstrated with one month's data from 30 EPN stations.

Acknowledgements
The authors thank IGS for data provision.

Funding
This study is sponsored by National Natural Science Foundation of China (42174029).

Abbreviations
Text for this section…

Availability of data and materials
Text for this section…

Ethics approval and consent to participate
Text for this section…

Competing interests
The authors declare that they have no competing interests.

Consent for publication
Text for this section…

Authors' contributions
Text for this section …

Authors' information

Text for this section. . .

Author details

[1]GNSS Research Center, Wuhan University, 129 Luoyu Road Wuhan 430079 China. [2]UPC-IonSAT / IEEC-UPC, UPC Mod.C3 Campus Nord UPC, c/ Jordi Girona 1-3 Barcelona Spain.

References

Caissy et al. (2012). Caissy M, Agrotis L, Weber G, Hernandez-Pajares M, Hugentobler U (2012). The International GNSS Real-Time service, GPS World, 6(23), 52-58.

Blanch (2003). Blanch J (2003) Using Kriging to bound satellite ranging errors due to the ionosphere. Ph.D. Thesis, Stanford University, California

Collins (2008). Collins, P. (2008) Isolating and estimating undifferenced GPS integer ambiguities. In Proceedings of the 2008 National Technical Meeting of The Institute of Navigation. 720-732.

Collins et al. (2010). Collins P, Bisnath S, Lahaye F, Héroux P (2010) Undifferenced GPS Ambiguity Resolution Using the Decoupled Clock Model and Ambiguity Datum Fixing. Navigation 57(2):123-135. https://doi.org/10.1002/j.2161-4296.2010.tb01772.x

Cressie and Hawkins (1980). Cressie N, Hawkins DM (1980) Robust estimation of the variogram: I. Mathematical Geology. 12(2), 115-125, doi:10.1007/BF01035243, 1980

Dow et al. (1996). Dow J, Martin-Mur T, Feltens J, García-martínez C, Bayona Perez M (1996) Orbital and other products of the international GPS service for geodynamics (IGS). Acta Astronautica, 38(4-8), 437-443. http://doi.org/10.1016/0094-5765(96)00016-1

Feltens and Schaer (1998). Feltens J, Schaer S (1998) IGS products for the ionosphere. In: Proceedings of the 1998 IGS analysis centers workshop, ESOC,Darmstadt, Germany

Gabor and Nerem (1999). Gabor, M. J., Nerem, R. S. (1999) GPS carrier phase ambiguity resolution using satellite-satellite single differences. In Proceedings of the 12th International Technical Meeting of the Satellite Division of The Institute of Navigation (ION GPS 1999). 1569-1578.

Ge et al. (2008). Ge M, Gendt G, Rothacher M, Shi C, Liu J (2008) Resolution of GPS carrier-phase ambiguities in Precise Point Positioning (PPP) with daily observations. J Geodesy 82(7):389-399. https://doi.org/10.1007/s00190-007-0187-4

Geng et al. (2019A). Geng J, Chen X, Pan Y, Zhao Q (2019) A modified phase clock/bias model to improve PPP ambiguity resolution at Wuhan University. J Geodesy 93(10):2053-2067. https://doi.org/10.1007/s00190-019-01301-6

Geng et al. (2019B). Geng J, Guo J, Chang H, Li X (2019) Toward global instantaneous decimeter-level positioning using tightly coupled multi-constellation and multi-frequency GNSS. J Geodesy 93(7):977-991. https://doi.org/10.1007/s00190-018-1219-y

Gong et al. (2018). Gong X, Gu S, Lou Y, Zheng F, Ge M, Liu J (2018) An efficient solution of real-time data processing for multi-GNSS network. J Geodesy 92(7):797-809. https://doi.org/10.1007/s00190-017-1095-x

Gu et al. (2021). Gu S, Dai C, Fang W, Zheng F, Wang Y, Zhang Q, Lou Y, Niu X (2021) Multi-GNSS PPP/INS tightly coupled integration with atmospheric augmentation and its application in urban vehicle navigation. J Geodesy 95(6):64. https://doi.org/10.1007/s00190-021-01514-8

Gu et al. (2015A). Gu S, Lou Y, Shi C, Liu J (2015A) BeiDou phase bias estimation and its application in precise point positioning with triple-frequency observable. J Geodesy 89(10):979-992. https://doi.org/10.1007/s00190-015-0827-z

Gu et al. (2015B). Gu S, Shi C, Lou Y, Liu J (2015B) Ionospheric effects in uncalibrated phase delay estimation and ambiguity-fixed PPP based on raw observable model. Journal of Geodesy, 89(5), 447-457. http://doi.org/10.1007/s00190-015-0789-1

Gu et al. (2020). Gu S, Wang Y, Zhao Q, Zheng F, Gong X (2020) BDS-3 differential code bias estimation with undifferenced uncombined model based on triple-frequency observation. J Geodesy 94(4):45. https://doi.org/10.1007/s00190-020-01364-w

Guerova et al. (2016). Guerova G, Jones J, Douša J, Dick G, Haan S de, Pottiaux E, Bock O, Pacione R, Elgered G, Vedel H, Bender M (2016) Review of the state of the art and future prospects of the ground-based GNSS meteorology in Europe. Atmos Meas Tech 9(11):5385-5406. https://doi.org/10.5194/amt-9-5385-2016

Hauschild and Montenbruck (2016). Hauschild A, Montenbruck O (2016) A study on the dependency of GNSS pseudorange biases on correlator spacing. Gps Solut 20(2):159-171. https://doi.org/10.1007/s10291-014-0426-0

Hernández-Pajares et al. (2009). Hernández-Pajares M, Juan J, Sanz J, Orús R, Garcia-Rigo A, Feltens J, Komjathy J, Schaer S, Krankowski A (2009) The IGS VTEC maps: a reliable source of ionospheric information since 1998. Journal of Geodesy. 83(3):263-275. doi:10.1007/s00190-008-0266-1

Hernández-Pajares et al. (2017). Hernández-Pajares, Manuel, David Roma-Dollase, Alberto García-Rigo, Denis Laurichesse, Michael Schmidt, Eren Erdogan, Yunbin Yuan, Zishen Li, José Ma. Gomez-Cama, Andrzej Krankowski, Haixia Lyu, Fabricio S. Prol (2017), Examples of IGS real-time Ionospheric information benefits: Space Weather monitoring, precise farming and RT-GIMs. In: IGS Workshop, Paris, France.

Romero et al. (2018). Ignacio (Nacho) Romero, C. Noll, K. MacLeod, D. Maggert, A. Rülke (2018) Infrastructure, Data Centers, Formats and Network: Status and Progress. In: IGS Workshop, Wuhan, China

Kouba and Héroux (2001). Kouba J, Héroux P (2001) Precise Point Positioning Using IGS Orbit and Clock Products. Gps Solut 5(2):12-28. https://doi.org/10.1007/pl00012883

Laurichesse et al. (2009). Laurichesse D, Mercier F, Berthias JP, Broca P, Cerri L (2009) Integer Ambiguity Resolution on Undifferenced GPS Phase Measurements and Its Application to PPP and Satellite Precise Orbit Determination. Navigation 56(2):135149. https://doi.org/10.1002/j.2161-4296.2009.tb01750.x

Laurichesse et al. (2013). Laurichesse D, Cerri L, Berthias J, Mercier F (2013) Real time precise GPS constellation and clocks estimation by means of a Kalman filter. Presented at the 26th International Technical Meeting of the Satellite Division of the Institute of Navigation, ION GNSS 2013, vol. 2, pp. 1155-1163

Li et al. (2017). Li M, Yuan Y, Wang N, Li Z, Li Y, Huo X (2017) Estimation and analysis of Galileo differential code biases. J Geodesy 91(3):279293. https://doi.org/10.1007/s00190-016-0962-1

Li et al. (2012). Li Z, Yuan Y, Li H, Ou J, Huo X (2012) Two-step method for the determination of the differential code biases of COMPASS satellites. J Geod 86(11):1059-1076. https://doi.org/10.1007/s00190-0120565-4

Liu et al. (2021). Liu Q, Hernández-Pajares M, Yang H, Monte-Moreno E, Roma-Dollase D, García-Rigo A, Li Z, Wang N, Laurichesse D, Blot A, Zhao Q, Zhang Q, Hauschild A, Agrotis L, Schmitz M, Wübbena G, Strze A, Krankowski A, Schaer S, Feltens J, Komjathy A, Ghoddousi-Fard R (2021) The cooperative IGS RT-GIMs: a reliable estimation of the global ionospheric electron content distribution in real time. Earth Syst Sci Data 13(9):45674582. https://doi.org/10.5194/essd-13-4567-2021

Lou et al. (2017). Lou Y, Gong X, Gu S, Zheng F, Feng Y (2017) Assessment of code bias variations of BDS triple-frequency signals and their impacts on ambiguity resolution for long baselines. Gps Solut 21(1):177-186. https://doi.org/10.1007/s10291-016-0514-4

Lou et al. (2015). Lou Y, Zheng F, Gu S, Wang C, Guo H, Feng Y (2015) Multi-GNSS precise point positioning with raw single-frequency and dual-frequency measurement models. GPS Solutions, 20(4), 849-862. http://doi.org/10.1007/s10291-015-0495-8

Luo et al. (2018). Luo X, Gu S, Lou Y, Xiong C, Chen B, Jin X (2018) Assessing the Performance of GPS Precise Point Positioning Under Different Geomagnetic Storm Conditions during Solar Cycle 24. Sensors, 18(6), 1784. http://doi.org/10.3390/s18061784

Luo et al. (2020). Luo X, Gu S, Lou Y, Cai L, Liu Z (2020) Amplitude scintillation index derived from C/N0 measurements released by common geodetic GNSS receivers operating at 1 Hz. J Geodesy 94(2):27. https://doi.org/10.1007/s00190-020-01359-7

Mannucci et al. (1998). Mannucci A, Wilson B, Yuan D, Ho C, Lindqwister U, Runge T (1998) A global mapping technique for GPS-derived ionospheric total electron content measurements. Radio Sci. 33 (3), 565-582, http://dx.doi.org/10.1029/97RS02707

Olivares-Pulido et al. (2021. Olivares-Pulido G, Hernndez-Pajares M, Lyu H, Gu S, Garca-Rigo A, Graffigna V, Tomaszewski D, Wielgosz P, Rapiski J, Krypiak-Gregorczyk A, Kamierczak R, Ors-Prez R (2021). Ionospheric tomographic common clock model of undifferenced uncombined GNSS measurements. Journal of Geodesy, 95(11), 1-13.

Psychas et al. (2021). Psychas D, Teunissen PJG, Verhagen S (2021) A Multi-Frequency Galileo PPP-RTK Convergence Analysis with an Emphasis on the Role of Frequency Spacing. Remote Sens-basel 13(16):3077. https://doi.org/10.3390/rs13163077

Psychas et al. (2020). Psychas D, Verhagen S, Teunissen PJG (2020) Precision analysis of partial ambiguity resolution-enabled PPP using multi-GNSS and multi-frequency signals. Adv Space Res-series 66(9):20752093. https://doi.org/10.1016/j.asr.2020.08.010

Rao and Mitra (1971). Rao CR, Mitra SK (1971) Generalized inverse of a matrix and its applications. New York.

Ren et al. (2019). Ren X, Chen J, Li X, Zhang X, Freeshah M (2019) Performance evaluation of real-time global ionospheric maps provided by different IGS analysis centers. Gps Solut 23(4):113. https://doi.org/10.1007/s10291-019-0904-5

Rovira-Garcia et al. (2015). Rovira-Garcia A, Juan JM, Sanz J, González-Casado G (2015) A Worldwide Ionospheric Model for Fast Precise Point Positioning. Ieee T Geosci Remote 53(8):4596-4604. https://doi.org/10.1109/tgrs.2015.2402598

Schaer (1999). Schaer S (1999) Mapping and predicting the Earth's ionosphere using the Global Positioning System. Ph.D. Thesis, University of Bern, Switzerland

Schönemann et al. (2011). Schönemann E, Becker M, Springer T (2011) A new Approach for GNSS Analysis in a Multi-GNSS and Multi-Signal Environment. J Geodetic Sci 1(3):204-214. https://doi.org/10.2478/v10156-010-0023-2

Shi et al. (2016). Shi C, Fan L, Li M, Liu Z, Gu S, Zhong S, Song W (2016) An enhanced algorithm to estimate BDS satellite's differential code biases. Journal of Geodesy, 90(2), 161-177. http://doi.org/10.1007/s00190-015-0863-8

Shi et al. (2012). Shi C, Gu S, Lou Y, Ge M (2012) An improved approach to model ionospheric delays for single-frequency Precise Point Positioning. Adv Space Res, 49(12):1698-1708. doi:10.1016/j.asr.2012.03.016

Shi et al. (2019). Shi C, Guo S, Gu S, Yang X, Gong X, Deng Z, Ge M, Schuh H (2019) Multi-GNSS satellite clock estimation constrained with oscillator noise model in the existence of data discontinuity. J Geodesy 93(4):515-528. https://doi.org/10.1007/s00190-018-1178-3

Shi et al. (2012B). Shi C, Zhao Q, Li M, Tang W, Hu Z, Lou Y, Zhang H, Niu X, Liu J (2012B) Precise orbit determination of Beidou Satellites with precise positioning. SCIENCE CHINA Earth Sciences. 55(7):1079-1086. doi:10.1007/s11430-012-4446-8

Snay and Soler (2008). Snay R, Soler T (2008) Continuously Operating Reference Station (CORS): History, Applications, and Future Enhancements. Journal of Surveying Engineering, 134(4), 95-104. http://doi.org/10.1061/(ASCE)0733-9453(2008)134:4(95)

Teunissen et al. (1999). Teunissen P, Joosten P, Tiberius C (1999) Geometry-free ambiguitysuccess rates in case of partial fixing. In: Proceedings of the 1999National Technical Meeting of The Institute of Navigation, SanDiego, CA. pp. 201-207.

Teunissen and Montenbruck (2017). Teunissen P, Montenbruck O (2017) Springer handbook of global navigation satellite systems. Cham: Springer.

Teunissen et al. (2010). Teunissen P, Odijk D, Zhang B (2010) PPP-RTK: Results of CORS Network-Based PPP with Integer Ambiguity Resolution. Journal of Aeronautics, Astronautics and Aviation. Series A, 2010, 42(4):223-229.

Wielgosz et al. (2021). Wielgosz, P., Milanowska, B., Krypiak-Gregorczyk, A. Jarmolowski,o W. (2021) Validation of GNSS-derived global ionosphere maps for different solar activity levels: case studies for years 2014 and 2018. GPS Solut 25, 103. https://doi.org/10.1007/s10291-021-01142-x

Yang et al. (2020). Yang Y, Mao Y, Sun B (2020) Basic performance and future developments of BeiDou global

navigation satellite system. Satell Navigation 1(1):1. https://doi.org/10.1186/s43020-019-0006-0
Yang (2019). Yang Y (2019) Resilient PNT Concept Frame. Journal of Geodesy and Geoinformation Science 2(3):17. https://doi.org/10.11947/j.jggs.2019.0301
YiChung (1997). YiChung C (1997) Real Time Implementation of the Wide Area Augmentation System for the Global Positioning System with an Emphasis on Ionospheric Modeling. PhD., Stanford University
Yigit and Gurlek (2017). Yigit CO, Gurlek E (2017) Experimental testing of high-rate GNSS precise point positioning (PPP) method for detecting dynamic vertical displacement response of engineering structures. Geomatics Nat Hazards Risk 8(2):112. https://doi.org/10.1080/19475705.2017.1284160
Yuan and Ou (2004). Yuan Y and Ou J (2004) A generalized trigonometric series function model for determining ionospheric delay. Progress in Natural Science, 14(11):1010-1014
Yuan et al. (2017). Yuan Yunbin, Huo Xingliang, Zhang Baocheng (2017) Research Progress of Precise Models and Correction for GNSS Ionospheric Delay in China over Recent Years. Acta Geodaetica et Cartographica Sinica, 46(10): 1364-1378. DOI: 10.11947/j.AGCS.2017.20170349
Zhang et al. (2013). Zhang H, Gao Z, Ge M, Niu X, Huang L, Tu R, Li X (2013) On the Convergence of Ionospheric Constrained Precise Point Positioning (IC-PPP) Based on Undifferential Uncombined Raw GNSS Observations. Sensors, 13(11):15708-15725. https://doi.org/10.3390/s131115708
Zhang et al. (2021). Zhang Z, Lou Y, Zheng F, Gu S (2021) ON GLONASS pseudo-range inter-frequency bias solution with ionospheric delay modeling and the undifferenced uncombined PPP. J Geodesy 95(3):32. https://doi.org/10.1007/s00190-021-01480-1
Zhao et al. (2018). Zhao Q, Wang Y, Gu S, Zheng F, Shi C, Ge M, Schuh H (2018) Refining ionospheric delay modeling for undifferenced and uncombined GNSS data processing. Journal of Geodesy, 56(3), 209-16. http://doi.org/10.1007/s00190-018-1180-9
Zhao et al. (2021). Zhao Q, Guo J, Liu S, Tao J, Hu Z, Chen G (2021) A variant of raw observation approach for BDS/GNSS precise point positioning with fast integer ambiguity resolution. Satell Navigation 2(1):29. https://doi.org/10.1186/s43020-021-00059-7
Zheng et al. (2017). Zheng F, Lou Y, Gu S, Gong X, Shi C (2017) Modeling tropospheric wet delays with national GNSS reference network in China for BeiDou precise point positioning. Journal of Geodesy, 20(2), 187-16. http://doi.org/10.1007/s00190-017-1080-4
Zumberge et al. (1997). Zumberge JF, Heflin MB, Jefferso DC, Watkins MM, Webb FH (1997) Precise point positioning for the efficient and robust analysis of GPS data from large networks. J Geophys Res. 102(B3):5005-5017
Zhang et al. (2022). Zhang Baocheng, Hou Pengyu, Zha Jiuping, Liu Teng (2021) A class of PPP-RTK functional models formulated at undifferenced and uncombined level
Zhang et al. (2020). Zhang Xiaohong, Hu Jiahuan, Ren Xiaodong (2020) New progress of PPP/PPP-RTK and positioning performance comparison of BDS/GNSS PPP. Acta Geodaetica et Cartographica Sinica, 49(9): 1084-1100. http://doi:10.11947/j.AGCS.2020.20200328